Gravitational Wave Polarization Analysis of GW170814

Robert C. Hilborn*

American Association of Physics Teachers, One Physics Ellipse, College Park, MD 20740

(Received ; published)

We use data from the GW170814 gravitational wave event detected by the three LIGO-VIRGO observatories to study the polarization properties of the gravitational waves. We find that within the LIGO-VIRGO 90% credible region of source sky locations, there is a range in which pure vector polarization is consistent with the observed amplitude ratios. Confirmation of a vector polarization component of gravitational waves would be a sign of post-general relativity physics.

DOI:

I. INTRODUCTION

The observation of the gravitational wave (GW) burst GW170814 by the three LIGO-VIRGO observatories [1] allows for a reasonably precise determination of the GW source location. More importantly, those observations permit a test of predictions for the polarization modes of the GWs, something not possible with the previous GW observations involving just the two LIGO observatories [2]. General relativity (GR) predicts that the GWs will exhibit only tensor polarization modes [1,3–6], an aspect of GR that has not been directly tested before. Any detection of non-tensorial polarization (that is, vector or scalar polarization modes) will be a signal of post-GR physics [7,8].

The comparisons of observations with GR polarization predictions need to consider the interplay among the GW source location (or equivalently, the GW wave propagation direction),

* rhilborn@aapt.org

the amplitudes and phases of the signals at the three observatories, the wave-front arrival times at the observatories, and the polarization properties of the GWs. The amplitudes and phase shifts depend, of course, on the orientation of the observatories' interferometer arms relative to the GW propagation direction and the GW polarization orientation.

Binary black hole GW signals such as GW170814 can be described in terms of three phases: (1) pre-merger inspiral, (2) merger, and (3) ring-down. We will focus on using the *pre-merger inspiral* data to analyze the results because linear GR provides explicit expressions (see Section III) for the orbital angle of inclination and polarization orientation angle dependence of the signals during the binary inspiral. During the merger and ring-down phases, the concomitant strong space-time curvature means that numerical GR is needed to analyze the polarization modes for those phases.

General metric theories of gravity indicate [7,9–13] that there are six possible polarization modes for GWs: two tensor polarization modes (the usual GR prediction), two vector polarization modes, and two scalar polarization modes. Using well known results (see, for example, Refs. [13,14]), we will show how to use both the standard tensor polarization modes and "non-standard" vector polarization modes that are permitted in more general metric theories of gravity, in a pure vector theory of gravity [15], and in electromagnetism-like (E&M-like) models of gravitational waves [16,17] to predict the ratios of the GW pre-merger amplitudes seen at the three observatories. (We will not treat the scalar "breathing" and longitudinal polarization modes here.) By focusing on the relative amplitudes among the three observatories, we eliminate the need to take into account the evolving GW amplitude and frequency during the pre-merger inspiral. More detailed analyses [18] show that the spins and masses of the orbiting objects determined from the inspiral data match the spins and masses determined from the full numerical GR analysis, giving further justification for relying on the inspiral phase for the polarization analysis.

We find that for the LIGO-VIRGO GW170184 maximum a posteriori sky location, tensor polarization can explain the observed amplitude ratios among the three observatories. This result is not surprising because the LIGO-VIRGO collaboration analysis assumed tensor polarization. However, as we shall see, for other sky locations consistent with the location uncertainty range, vector polarization models cannot be ruled out.

The sky location of the GW source can be reasonably well determined from the arrival-time delays of the gravitational wave-front at the three observatories. However, the observed delay

times may be affected by phase shifts between the detectors' responses to the polarization modes. Generally, those phase shifts are different for the different observatories and are not known a priori [19]. In turn, inferences about the polarization of the gravitational waves depends on the source location. We explore a range of sky locations to study the interdependence of these parameters.

Here we focus on the GW170814 binary black hole gravitational wave observations recorded at the Hanford, Livingston, and VIRGO gravitational wave observatories [1] in terms of the GW polarization orientation angle and the binary orbital angle of inclination. It turns out to be important to consider the full range of those angles [20].

The complex interplay among the GW wave source and polarization parameters, the detector parameters, and the observations ought to encourage us to undertake a detailed full-parameter fit, considering priors of the various parameters and their measurement error distributions and appropriate weighting factors [21,22], just what the LIGO-VIRGO collaboration carried out for its GW detection events. The strategy in this paper, however, is to take a step-wise approach that exposes the physics of the dependence of the GW signals on the propagation direction, the orbital angle of inclination, the polarization orientation angle, and the detectors' geometry. We shall see that this approach yields results that are consistent with the LIGO-VIRGO results [1] but they also indicate that the data from GW170814 cannot rule out a vector polarization component for GWs.

II. GRAVITATIONAL WAVE AND DETECTOR GEOMETRY

In this section we introduce the orbital angle of inclination, the polarization orientation angle, and a set of unit vectors to specify the geometry of the detector orientation, all of which affect the GW signals seen by the LIGO-VIRGO observatories.

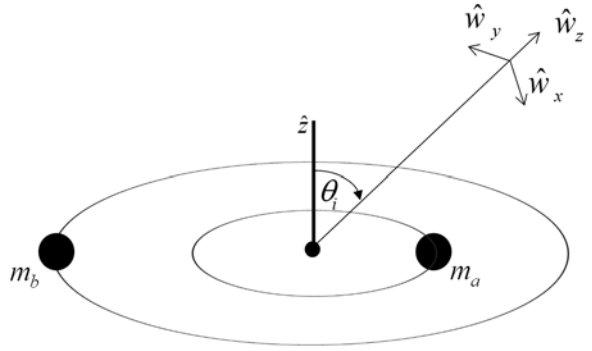

FIG. 1. A perspective view of the orbits for masses m_a and m_b, showing the definition of the angle of inclination θ_i and the gravitational wave unit vectors. The unit vector $\hat{z}$ is perpendicular to the plane of the orbit and parallel to the system's orbital angular momentum. The gravitational wave unit vector $\hat{w}_z$ points from the binaries' center of mass to the observation point. $\hat{w}_x$ lies in the $\hat{z}$-$\hat{w}_z$ plane. $\hat{w}_y$ is perpendicular to that plane.

Figure 1 shows the definition of the binary orbit's angle of inclination θ_i, the angle between $\hat{w}_z$, pointing from the source to the observation point, and $\hat{z}$ normal to the orbital plane. The vector $\hat{w}_x$ lies in the $\hat{z}$-$\hat{w}_z$ plane while $\hat{w}_y$ is perpendicular to that plane.

In this paper, we will focus on the Hanford (*H*), Livingston (*L*), and VIRGO (*V*) observatories of the LIGO-VIRGO collaboration. The detector arms' orientations are specified in terms of unit vectors $\hat{d}_x$ and $\hat{d}_y$, which define the detector plane (with d = *H*, *L*, or *V*). The local vertical direction is along $\hat{d}_z$. The geometry of the GW observatories is usually specified by the latitude and longitude of the vertex of the interferometer arms and unit vectors giving the orientation of the two interferometer arms in the plane perpendicular to the local vertical.

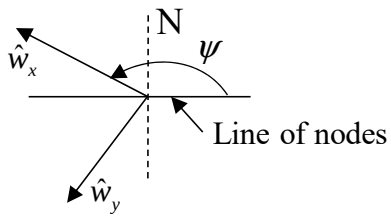

FIG. 2. The definition of the gravitational wave polarization orientation vector ψ. $\hat{w}_z$ (not shown) points up and out of the page. The Line of nodes is the intersection of the wave front $\left(\hat{w}_x\text{-}\hat{w}_y\right)$ plane and Earth's equatorial plane. The dashed line is perpendicular to Earth's equatorial plane.

As mentioned previously, we also need to take into account the orientation of the GW polarization axes relative to the detector arms. The orientation of the GW polarization may be specified by an angle ψ measured relative to the "Line of nodes" defined by the intersection of the wave front $(\hat{w}_x\text{-}\hat{w}_y)$ plane and Earth's equatorial plane. See Fig. 2.

To calculate the GW detector signal, we also need to know the direction of propagation of the GW. The propagation direction vector that passes through the center of Earth first hits Earth's surface at a point whose location we will specify in terms of latitude and longitude. In what follows, we will discuss the standard method used to find the latitude and longitude of that point for a short GW burst.

Given the information on the orientation of the GW detectors, the GW wave propagation direction, and the polarization orientation, calculating the effects of the gravitational wave polarization for the LIGO-VIRGO detectors is a straightforward matter of geometry.

III. ANTENNA PATTERNS AND DETECTOR SIGNALS

In this section we summarize how to use the vectors introduced in the previous section to find the GW detectors' responses to GWs. We will first give the tensor polarization properties associated with the standard linear form of GR. We then show how those results are modified if we use a GW vector polarization model.

Each detector's strain signal can be written as the sum of the contributions of two polarization modes [5,14,20,23–25]

$$h_D(t) = h_{D1}(t)\cos(\omega t) + h_{D2}(t)\sin(\omega t), \tag{1}$$

where

$$h_{D1,2}(\theta_i,\psi,t) = a(t)\, f_{1,2}(\theta_i) F_{1,2}(\hat{w},\hat{d})\,. \tag{2}$$

In Eqs. (1) and (2), we have $D = H$, L, or V and $a(t)$ is a slowly varying amplitude, which depends on the distance from the source to the observation point and the source properties such as orbital frequency and mass separation. ω is the GW frequency (twice the binary orbital frequency), which also varies slowly in time during the inspiral. The functions $f_{1,2}(\theta_i)$ give the dependence on the orbital angle of inclination, while the antenna pattern functions $F_{1,2}(\hat{w},\hat{d})$ provide the dependence on the wave propagation direction, the polarization orientation angle, and the detector geometry.

For the inspiral phase, we write the detector signal in terms of an overall amplitude and phase:

$$h_D(t) = A_D(\theta_i,\psi,t)\cos(\omega t + \Phi_D)\ , \tag{3}$$

with

$$A_D = \sqrt{h_{D1}^2 + h_{D2}^2}\ . \tag{4}$$

The phase angle is given by

$$\Phi_D = \tan^{-1}\left[-h_{D2}\,/\,h_{D1}\right]. \tag{5}$$

A. Tensor Polarization

In GR's treatment of gravitational waves [3,4], there are two tensor polarization modes, "plus" (+) and "cross" (×), with amplitudes A_+ and $A_\times$. The antenna pattern functions are [23]

$$\begin{aligned} F_+(\hat{w},\hat{d}) &= \tfrac{1}{2}\left[\left(\hat{w}_x\cdot\hat{d}_x\right)^2 - \left(\hat{w}_x\cdot\hat{d}_y\right)^2 - \left(\hat{w}_y\cdot\hat{d}_x\right)^2 + \left(\hat{w}_y\cdot\hat{d}_y\right)^2\right] \\ F_\times(\hat{w},\hat{d}) &= \left(\hat{w}_x\cdot\hat{d}_x\right)\left(\hat{w}_y\cdot\hat{d}_x\right) - \left(\hat{w}_x\cdot\hat{d}_y\right)\left(\hat{w}_y\cdot\hat{d}_y\right). \end{aligned} \tag{6}$$

The inclination angle dependence for a binary orbit GW source is given by [12,26]

$$\begin{aligned} f_+(\theta_i) &= (1+\cos^2\theta_i)/2 \\ f_\times(\theta_i) &= -\cos\theta_i\ . \end{aligned} \tag{7}$$

The dependence on the polarization angle is via the GW vector $\hat{w}$. For a periodic GW source, there is a 90° temporal phase difference between the two polarization modes.

B. Vector Polarization

As mentioned previously, in generalized metric theories of gravity, GWs may have a mix of tensor, vector, and scalar polarization modes. In a pure vector theory of gravity [15] and in an E&M-like (vector) model of GWs [16,17], the GW waves have vector polarization components (exactly like the description of polarization for E&M waves). For a simply periodic wave source, the two polarization modes have a temporal phase difference of 90°.

The vector model antenna pattern response functions are [23]

$$\begin{aligned} F_x(\hat{w},\hat{d}) &= \left(\vec{w}_z \cdot \vec{d}_x\right)\left(\vec{d}_x \cdot \vec{w}_x\right) - \left(\vec{w}_z \cdot \vec{d}_y\right)\left(\vec{d}_y \cdot \vec{w}_x\right) \\ F_y(\hat{w},\hat{d}) &= \left(\vec{w}_z \cdot \vec{d}_y\right)\left(\vec{d}_y \cdot \vec{w}_y\right) - \left(\vec{w}_z \cdot \vec{d}_x\right)\left(\vec{d}_x \cdot \vec{w}_y\right). \end{aligned} \tag{8}$$

In an E&M-like model [16,17] of GWs, the pre-merger dependences on the angle of inclination for a binary orbit GW source are

$$\begin{aligned} f_x(\theta_i) &= \sin 2\theta_i \\ f_y(\theta_i) &= -2\sin\theta_i \,. \end{aligned} \tag{9}$$

It is important to note that the antenna pattern functions in Eqs. (6) and (8) will hold for any gravitational wave theory since they are purely geometric expressions of what we mean by tensor polarization and vector polarization, respectively.

We will be interested in looking at ratios of amplitudes for the different observatories, for example A_V / A_L, and phase differences, for example $\Phi_V - \Phi_L$, as functions of the angles θ_i and ψ. As mentioned previously, using those ratios removes the effects of the time-varying frequency and amplitude during the pre-merger inspiral. Our only assumption is that the relative amplitudes and phases of the polarization modes do not change significantly during the binary inspiral. Comparison with the GW170814 observations will then in principle give us information about possible values of θ_i and ψ consistent with those observations. Ref. [27] describes a similar approach for gravitational wave polarization analysis.

To calculate the various scalar products in Eqs. (6) and (8), it is helpful to express each of the vectors in terms of an Earth-fixed coordinate system with $\vec{z}_E$ running from the South pole towards the North pole, $\vec{x}_E$ running from the center of Earth along the prime meridian (which intersects the surface at 0° longitude) and $\vec{y}_E$ forming a right-handed Cartesian coordinate system with $\vec{x}_E$ and $\vec{z}_E$. The components of each of the detector unit vectors in the Earth-fixed system are available from the LIGO-VIRGO collaboration [25,28]. The gravitational wave unit vectors can be expressed in terms of the Earth-fixed unit vectors by using the source latitude and longitude at the time of the event (or equivalently, the source's Right Ascension and declination) and the unknown polarization orientation angle ψ. For an alternative approach to dealing with this geometry, see Refs. [29,30].

IV. GW SOURCE LOCATION

In this section we review how to use the observed wave-front arrival-time delays among the three observatories to determine the celestial coordinates of the gravitational wave source. We assume that the GW signal duration is short (in practice from a few tenths of a second to a few tens of seconds for recent observations) so the source location relative to the rotating and orbiting Earth does not change significantly during the wave observation time.

We denote the position of the Hanford observatory relative to the Livingston observatory as $\vec{r}_{LH}$ and the analogous position of VIRGO as $\vec{r}_{LV}$. Given those vectors, it is easy to see that the arrival-time delays are given by

$$\Delta t_{LH} = \hat{w}_z\left(\theta_{lat}, \phi_{long}\right) \cdot \vec{r}_{LH} \,/\, c \tag{10}$$

$$\Delta t_{LV} = \hat{w}_z\left(\theta_{lat}, \phi_{long}\right) \cdot \vec{r}_{LV} \,/\, c\,, \tag{11}$$

where θ_{lat} and ϕ_{long} are the latitude and longitude of the GW source at the time of the event. The gravitational wave speed is assumed to be the usual speed of light. The GW propagation unit vector can be expressed as

$$\hat{w}_z\left(\theta_{lat}, \phi_{long}\right) = -\left(\cos\theta_{lat}\cos\phi_{long}\,\hat{x}_E + \cos\theta_{lat}\sin\phi_{long}\,\hat{y}_E + \sin\theta_{lat}\,\hat{z}_E\,\right). \tag{12}$$

Eqs. (10) and (11) provide two equations for the two unknown angles θ_{lat} and ϕ_{long}.

We will now employ the expressions given above to extract information about the GW source location based on the observations of GW170814 described in Ref. [1]. Using the reported gravitational wave-front arrival-time delays, $\Delta t_{LH} = 8$ ms and $\Delta t_{LV} = 14$ ms, for Livingston-Hanford and Livingston-VIRGO respectively, and the relative position vectors $\vec{r}_{LH}$ and $\vec{r}_{LV}$, we find for the source latitude and longitude $\theta_{lat} = 49.7^{\circ}$ S and $\phi_{long} = 77^{\circ}$ W at the time of the event. The full parameter estimation of Ref. [1] constrains the position to a 90% credible area of 60 deg^2 with a maximum a posteriori position of right ascension RA = $03^{h}11^{m}$ and declination dec = $-44°57^{m}$ (J2000). The GW170814 Fact Sheet [31] states that the maximum a posteriori location is equivalent to $\theta_{lat} = 45^{o}$ S and $\phi_{long} = 73^{\circ}$ W. (See Ref. [19] for a discussion of how source localization can be improved by taking into account GW polarization and assumptions about the astrophysical distribution of sources.)

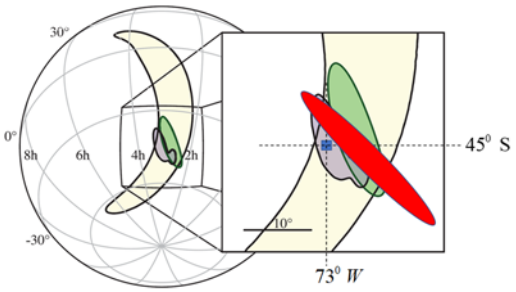

FIG. 3. Based on Fig. 3 (CC BY 3.0) of Ref. [1], this figure shows the possible locations of the GW170814 source in equatorial (celestial) coordinates. The inset is a gnomonic projection. The contours represent the 90% credible regions. The light (yellow) shading is the localization using only the two LIGO sites. The intermediate (green) shading is the rapid localization results using data from all three observatories, while the asymmetric (purple) area with a lobe is the full parameter estimation localization [1]. The inset's filled square indicates approximately the maximum a posteriori source location: RA 03^{h} 11^{m}, dec – 44^{o} 57^{m}. The dark (red) oval indicates the approximate range of source locations, discussed later, for which a vector polarization model can explain the observations.

Figure 3 indicates the LIGO-VIRGO asymmetric 90% credible region for the source location, based on data from all three observatories. The longitude uncertainty is about $\pm 5^{o}$ (90% credible limits) while the latitude uncertainty is about $\pm 7^{o}$. Those uncertainties are consistent with an arrival-time uncertainty about ± 1 ms. Within those uncertainties, the latitude and longitude results found here agree with the GW170814 maximum a posteriori source location mentioned previously.

The main point of this section is that the GW source location parameters are sensitive to the arrival-time delays among the three observatories. Note that the recently observed binary neutron star event GW170817 [32] is a special case because the sky location could be determined rather precisely due to the independent observations of electromagnetic emissions from the colliding neutron stars [32,33].

V. POLARIZATION, ORBITAL INCLINATION, AND RELATIVE AMPLITUDES

We now use a specified source location and determine what limits (if any) can be placed on the orbital angle of inclination θ_i and the polarization orientation angle ψ. We will look at the predicted GW signal amplitude ratios (Hanford/Livingston and VIRGO/Livingston) and the corresponding signal phase differences as a function of those angles and see, for both tensor and vector polarization models, what ranges are consistent with the observations.

There are several complications in this analysis. First, Eqs.(1) and (2) come from the linear version of GR or the E&M-like model of GWs, both of which are restricted to the pre-merger GW signals emitted before the two black holes coalesce. We expect that the polarization properties of the GWs might change during the merger and ring-down phases due to the strong space-time curvature produced during those phases, an effect similar to the time delays caused by such curvature [34]. Thus, we focus on the pre-merger inspiral. Extensions to the merger and ring-down phases are discussed in Section VIII.

The second complication arises because the numerical GR and template models for the strain signals plotted in Fig. 1 of Ref. [1] (hereafter denoted as GW170814-Fig. 1) are "whitened" by dividing the physical strain Fourier components by the frequency-dependent noise amplitude spectral density, different for each of the three observatories. Thus, to extract the ratios of the physical strains from the published numerical GR and template data, we need to remove the whitening. This can be done using the noise amplitude spectral density data found in Fig. 2 of

Ref. [1] for each of the three observatories. We use the relative noise amplitudes in the 55-65 Hz range since that is the appropriate range for the GW170814 pre-merger inspiral.

A third complication arises because selection of the maximum a posteriori waveform templates shown in GW170814-Fig. 1 is dominated by the merger part of the observed signal due to its considerably larger signal-to-noise ratio (SNR). Conversely, the pre-merger part of the waveform template is less well-determined because the SNR during that phase is much smaller. Hence, the amplitude ratios determined from the inspiral stage have an accompanying (and difficult to specify) uncertainty range. Lacking other data, we will use the amplitude ratios determined as described above, with the whitening of the displayed data taken into account, to demonstrate how one would carry out this analysis if high quality, small uncertainty amplitude ratios become available.

The fourth complication comes from possible spin-orbit and spin-spin effects if the black holes are rotating [26]. These effects will cause the orbital angular momentum direction (which is of course perpendicular to the plane of the binary orbits) to precess about the total angular momentum direction. This precession implies that the orbital angle of inclination will be modulated as a function of time, leading to a modulation in the ratio of the polarization mode amplitudes and consequently of the signal amplitudes at the detectors. Furthermore, the total angular momentum of the binary system will change because the GWs themselves carry away angular momentum. For simplicity's sake we will ignore those complications in this analysis. A treatment of GWs emitted by binary black holes with spin is given in Ref. [35].

We will first use the LIGO-VIRGO GW170814 maximum a posteriori source location $\left(\theta_{lat} = 45^{\circ}\ \text{S and}\ \phi_{long} = 73^{\circ}\ \text{W}\right)$ to examine both the standard GR tensor polarization and vector polarization model predictions for the amplitude ratios. Later we will explore how the results vary when the source location changes.

A. Tensor polarization model

First let's look at the linear GR (tensor polarization) prediction for the Livingston observatory signal as a function of the orbital angle of inclination θ_i and the polarization orientation angle ψ, assuming the LIGO-VIRGO maximum a posteriori latitude and longitude values for the GW source location. This analysis will help build our intuition about what to expect for the ratios of amplitudes among the various observatories.

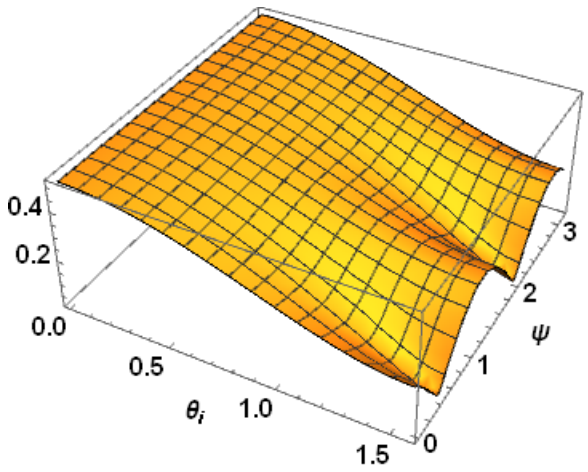

FIG. 4. The linear GR prediction for the Livingston observatory strain signal amplitude (arbitrary units) as a function of the orbital angle of inclination θ_i and the polarization angle of orientation ψ, both in radians. The amplitude is symmetric about the $\theta_i = \pi/2$ line (not shown).

For small angles of inclination (that is, the observation direction is nearly perpendicular to the plane of the binary orbit), linear GR theory (see Eq. (7)) predicts equal amplitudes for the cross and plus polarization modes. Since the temporal phase difference between the modes is $\pi/2$, we have the equivalent of "circular polarization," for which the amplitude is independent of the polarization angle ψ as illustrated in Fig. 4.

As $\theta_i \to \pi/2$, the cross polarization mode amplitude $A_\times$ goes to zero, leaving only the plus polarization. We see from Fig. 4 that the amplitude then has a strong dependence on ψ with a periodicity of $\pi/2$, characteristic of the tensor modes of quadrupole radiation. (For vector polarization, the periodicity is π.) The amplitude graphs for the Hanford and VIRGO signals are similar. Also note that the maximum amplitude occurs for θ_i near 0 and π, so there may be an observational bias [36] for "face-on" binary orbits. That is, for binaries with identical masses at identical distances, the observations will favor those orbits that are face-on versus those that are "edge-on" ($\theta_i \approx \pi/2$).

Let's now turn our attention to the amplitude ratios for the different observatories since those ratios are expected to be independent of the time-dependent frequency and amplitude of the GW, at least during the inspiral phase. As mentioned previously, those ratios allow us to probe the

polarization properties of the GWs, an aspect not possible to explore before the first "three-observatory" data from GW170814.

Using the LIGO-VIRGO numerical GR results (GW170814-Fig. 1) as reasonable representations of the GW signal (taking into account the complications mentioned previously) and removing the whitening using data from Fig. 2 of Ref. [1], we find that the pre-merger inspiral physical strain amplitude ratios are $H / L \approx 1$ and $V / L \approx 0.8$, both with an estimated uncertainty of about $\pm 20\%$. (The results that follow do not depend critically on the uncertainty range.) Those ratios are in agreement with those stated in the LIGO-VIRGO GW170814 Fact Sheet [31].

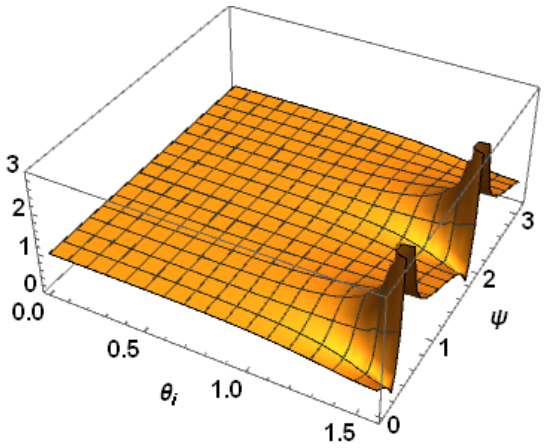

FIG. 5. A plot of the Hanford-to-Livingston GW signal amplitude ratio as a function of the orbital angle of inclination θ_i and the polarization orientation angle ψ, both in radians. The "spikes" occur in regions where the Livingston amplitude is very small.

To get a sense of how the amplitude ratios depend on the orbital angle of inclination and the polarization orientation angle, we plot the tensor polarization model predictions for the *H/L* ratio in Fig. 5. We see that for $0 \le \theta_i < 1$ the ratio is about 1, consistent with the estimates given previously. However, for $\theta_i \to \pi / 2$, where the plus polarization mode dominates, we find ratios that are strongly dependent on the polarization orientation angle ψ.

To compare the predicted amplitude ratios quantitatively to those observed for GW170814, it is helpful to look at contour maps of the ratios as shown in the figures below. In what follows, we assume that the Hanford/Livingston amplitude ratio falls in the range [0.8, 1.2] and the VIRGO/Livingston ratio is the range [0.64, 0.96], both representing a ± 20 % uncertainty range.

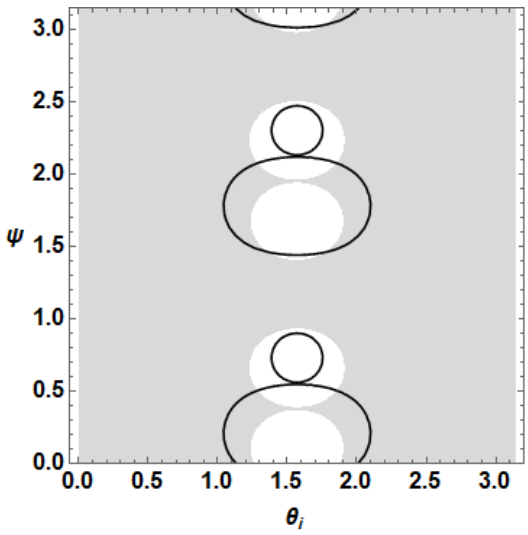

FIG. 6. A contour plot of the linear GR tensor polarization model calculation of the VIRGO/Livingston and Hanford/Livingston GW strain signal amplitude ratios that fall within the uncertainty range of the pre-merger observations, plotted as a function of θ_i and ψ, both in radians. Source location: 45° S, 73° W. Solid line contours bound the *V/L* ratio range. The shaded (gray) area indicates the *H/L* ratio range. The white areas are regions where the calculated *H/L* ratios are outside the uncertainty range.

Figure 6 shows the linear GR calculation of the range of orbital inclination and polarization orientation angles consistent with the observed *H/L* and *V/L* amplitude ratios during the pre-merger inspiral. In this case, the region outside the solid curves indicates the range of θ_i and ψ that gives ratios consistent with the *V/L* amplitude observations (taking into account the range of uncertainty). The shaded region indicates the angular range that gives *H/L* amplitude ratios consistent with the observations. We see that there is a wide range of angles for which the ratio ranges overlap and only a small range near $\theta_i \approx \pi/2$ for which no overlap occurs. Thus, we conclude that the tensor polarization model can account for the observations for a significant range of θ_i and ψ. As mentioned previously, this result should not be surprising since the LIGO-VIRGO analysis assumed pure tensor polarization. Let us now examine vector model predictions.

B. Vector polarization model

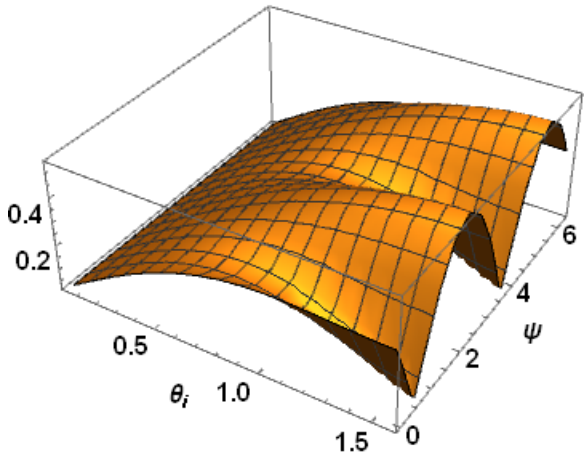

FIG. 7. The vector polarization model predictions for the Livingston GW strain signal amplitude (arbitrary units) as a function of the orbital angle of inclination θ_i and the polarization orientation angle ψ, both in radians. Source location: 45° S, 73° W. The amplitude is symmetric about the $\theta_i = \pi/2$ line (not shown).

Figure 7 shows a plot of the Livingston observatory GW strain signal amplitude as predicted by the vector polarization model. Note that for small values of the orbital angle of inclination θ_i, the amplitude is largely independent of the polarization orientation angle ψ: in this range the predicted GW emission is approximately circularly polarized, so there is no significant orientation angle dependence. Note also that the amplitude goes to zero as $\theta_i \to 0$: in the vector model there is no gravitational wave emission perpendicular to the plane of the orbit, in contrast to the GR tensor polarization model for which the power emission is maximum in that direction. So, in a pure vector polarization model, there is an observational bias for edge-on orbits.

As $\theta_i \to \pi/2$, the vector polarization "*x*-mode" amplitude goes to zero, and the emission is almost completely linearly polarized. In that case, the amplitude is strongly dependent on ψ and repeats every π radians, characteristic of vector linear polarization (like E&M linear polarization). The Hanford and VIRGO amplitudes are similar but with shifts in their ψ dependence.

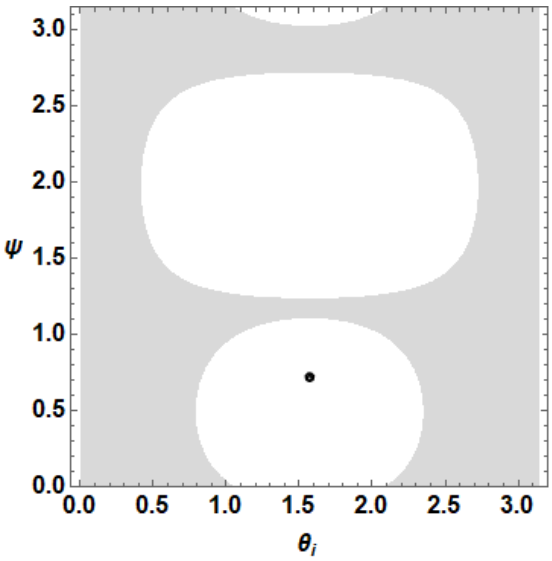

FIG. 8. A contour plot indicating the vector polarization model calculation of the VIRGO/Livingston and Hanford/Livingston GW strain signal amplitude ratios that fall within the range of the pre-merger inspiral observations (taking into account the uncertainty range) plotted as a function of θ_i and ψ, both in radians. Source location: 45° S, 73° W. Solid line contours indicate the *V/L* angular ranges that give amplitude ratios consistent with the observations. The shaded area indicates the *H/L* ratio range. The white areas are regions for which the calculated *H/L* ratios are outside the range of uncertainty.

Now let's use a contour plot to look at the amplitude ratios. We see from Fig. 8 that the region near $\theta_i \approx \pi/2$ and $\psi \approx 0.7$, for which the vector model predictions agree with the *V/L* amplitude ratio, is very small and that there is no overlap with the regions consistent with *H/L* ratio range. Hence, we conclude that the vector polarization model cannot account for the observed pre-merger amplitude ratios for the LIGO-VIRGO maximum a posteriori GW source location.

VI. CHANGING THE GW SOURCE LOCATION

We now look at how the amplitude ratio predictions vary if we change the GW source location. As noted previously, there is a substantial range of source locations consistent with the uncertainties in the wave-front arrival times at the detectors. After exploring several combinations of source latitude and longitude, we found a band of source locations (see the oval in Fig. 3) for which a vector polarization model gives results in agreement with the observed amplitude ratios.

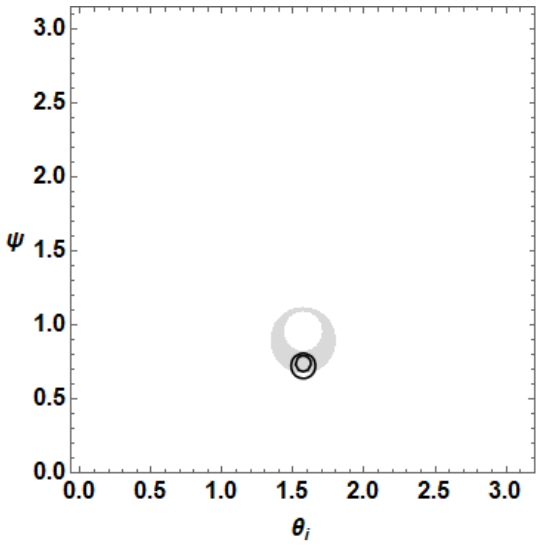

FIG. 9. A contour plot indicating the vector polarization model calculation of the VIRGO/Livingston and Hanford/Livingston GW strain signal amplitude ratios that fall within the uncertainty range of the pre-merger observations plotted as a function of θ_i and ψ, both in radians. Source location: 40° S, 71.5° W. Solid line contours indicate the *V/L* ratio range. The shaded (gray) area indicates the *H/L* ratio range.

Figure 9 shows the predicted amplitude ratio results for the vector polarization model with a source location 40° S, 71.5° W. In this case, the region between the two solid line contours is consistent with the observed *V/L* amplitude ratios. Note that we now have overlap regions near $\theta_i \approx \pi/2$ rad and $\psi \approx 0.7$ rad. The pattern repeats for $\psi \rightarrow \psi + \pi$ (not shown). Hence, we conclude that vector polarization contributions cannot be excluded for this source location.

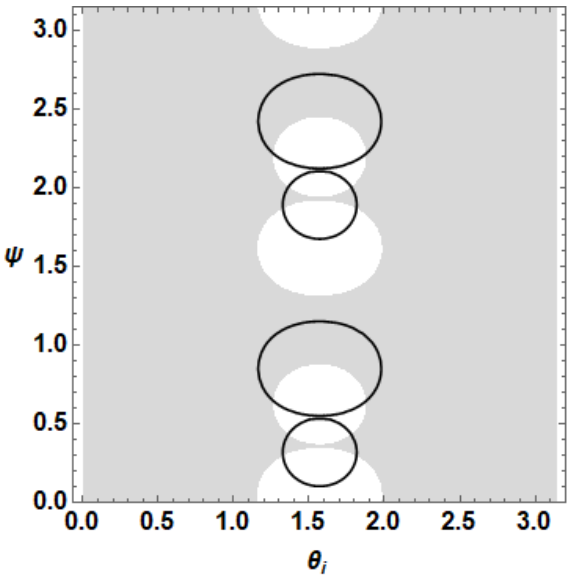

FIG. 10. A contour plot indicating the tensor polarization model calculations for the VIRGO/Livingston and Hanford/Livingston GW strain signal amplitude ratios that agree with the pre-merger observations (taking into account the range of uncertainty) plotted as a function of θ_i and ψ, both in radians. Source location: 40° S, 71.5° W. Solid line contours indicate the angular range that gives *V/L* ratios consistent with the observations. The shaded (gray) area indicates the *H/L* ratio range.

Figure 10 shows analogous results for the tensor polarization model. We see that there is a wide range of angles, except for small regions near $\theta_i \approx \pi/2$, for which the tensor polarization model predictions agree with the observed pre-merger amplitude ratios. Note that the pattern repeats when $\psi \to \psi + \pi/2$. This pattern for the new source location is much like the one shown in Fig. 6.

The dark (red) oval in Fig. 3 gives the approximate set of source locations that give rise to vector polarization amplitude ratio predictions in agreement with the observations. These range from roughly 33° S, 77° W to 53° S, 50° W with a longitude range of approximately $\pm 2^\circ$ for each latitude.

To illustrate how the contour plots vary with source locations within the Fig. 3 oval, we show a contour plot for one more source location for which both the tensor and vector polarizations account for the observed amplitude ratios.

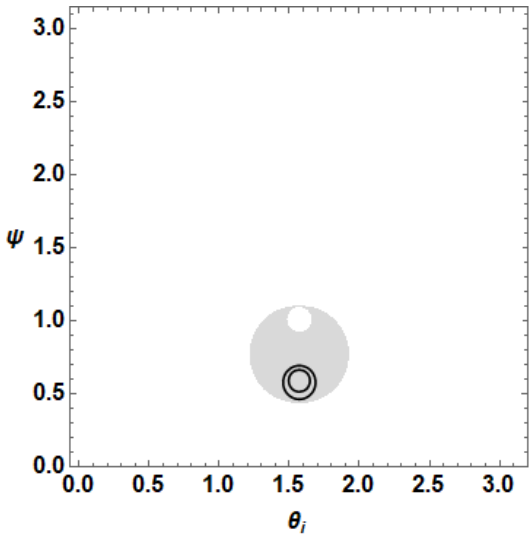

FIG. 11. A contour plot indicating the vector polarization model calculation of the VIRGO/Livingston and Hanford/Livingston GW strain signal amplitude ratios that fall within the uncertainty range of the pre-merger observations plotted as a function of θ_i and ψ, both in radians. Source location: 46° S, 65.5° W. Solid line contours indicate the *V/L* ratio range. The shaded area indicates the *H/L* ratio range.

Figure 11 shows that the vector polarization predictions for the observed amplitude ratios for the stated source location are consistent with the amplitude ratio observations. We conclude that, surprisingly, the vector polarization model can account for the observed pre-merger amplitude ratios for GW source locations within a range that overlaps and extends beyond the LIGO-VIRGO GW170814 90% credible region, but only for relatively small ranges of θ_i and ψ. (The tensor polarization model also accounts for observed amplitude ratios for those source locations in the oval area of Fig. 3.) In other words, the observed amplitude ratios do not rule out vector contributions to the GW polarization. Based on a detailed analysis of an E&M-like model of GWs from orbiting binaries [17], we anticipate that in such a model the vector polarization contribution to the GW amplitude will be about 1/4 the contribution from the linear GR tensor model for a given set of binary masses. Of course, the vector contribution may be different for other gravitational theories [15].

For the range of source locations studied here, we have not found any for which the tensor and vector polarization results both agree with observed amplitude ratios in the same range of θ_i and

ψ. If that situation obtains more generally, we would need to conclude that the GWs have only tensor polarization modes or only vector polarization modes. Observations of other GW events by the three observatories with presumably different values of θ_i and ψ will, in principle, allow us to sort out these possibilities.

VII. PHASE DIFFERENCES

The observed amplitude ratios are intimately tied to the GW source sky location,, the orbital angle of inclination, and the polarization orientation as shown in the previous section. The signals also depend on phase differences of the GW strain amplitudes at the observatories due to the orientations of the detectors' arms relative to the GW polarization and propagation directions. We shall call those phases "intrinsic phases" to distinguish them from phases associated with different arrival times at the three detectors.

We now examine the intrinsic phase differences between the VIRGO and Livingston signals and the Hanford and Livingston signals. In the convention used here (see Eq.(3)), a negative phase difference implies an additional time delay between the two sites beyond the time-of-flight delay. We restrict the phase differences to lie in the range $[-\pi, \pi]$.

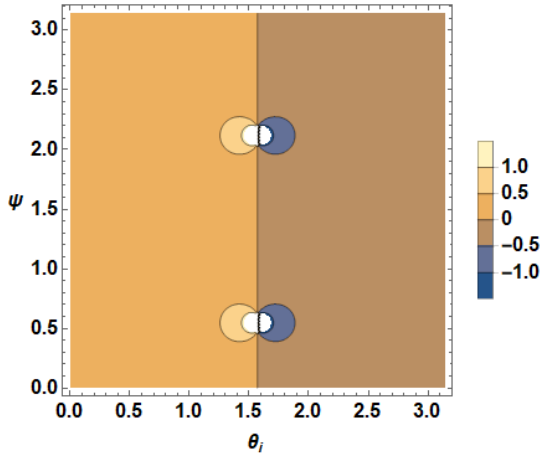

FIG. 12. A contour plot of the tensor model calculation of the VIRGO-Livingston phase difference predictions (in radians) as a function of the orbital angle of inclination θ_i and the polarization orientation angle ψ (both in radians). Source location: 45° S, 73° W.

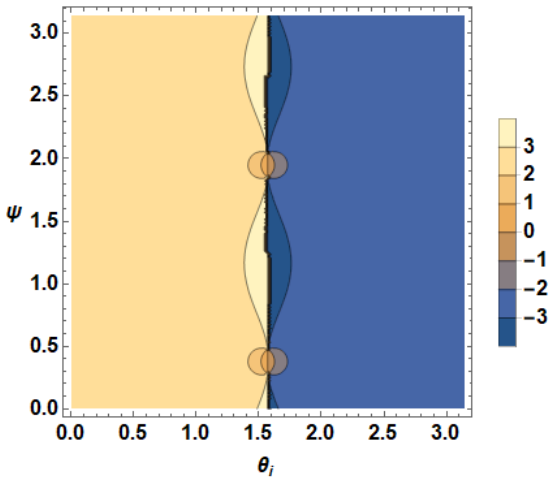

FIG. 13. A contour plot of the Hanford-Livingston tensor model phase difference predictions (in radians) as a function of the orbital angle of inclination and the polarization orientation angle (both in radians). Same source location as Fig. 12.

The tensor model intrinsic phase difference predictions are shown in Figs. 12 and 13 for the source location 45° S, 73° W, the LIGO-VIRGO maximum a posteriori source location. The pattern repeats for $\psi \rightarrow \psi + \pi / 2$. Fig. 12 indicates a small VIRGO-Livingston phase shift over most of the range of angles. For example, a – 0.3 radian phase shift corresponds to a time delay of about 0.8 ms for a gravitational wave frequency of about 60 Hz (see GW170814-Fig. 1). That shift would be difficult to observe because it is well within the range of uncertainty of the arrival-time delays.

What do we expect for the Hanford-Livingston phase difference? By design, the Hanford-Livingston interferometer arms are approximately aligned with $\hat{H}_x \approx -\hat{L}_y$ and $\hat{H}_y \approx \hat{L}_x$. Hence, Eqs. (6) and (8) indicate that we should expect $\pm\pi$ for the overall intrinsic phase shift. However, the alignment is not exact. The angle between $\hat{H}_x$ and $-\hat{L}_y$ is about 24° and between $\hat{H}_y$ and $\hat{L}_x$ about 13°. So the phase shifts will differ from π and are likely to depend significantly on θ_i and ψ as seen in Fig. 13.

GW170814-Fig. 1 shows that the Hanford strain signal relative to the Livingston strain signal data are consistent with an intrinsic phase of about $\pm\pi$ and an arrival-time delay of about 8 ms during the pre-merger regime. (The effect of the frequency-dependent signal whitening on the observed time delay needs to be examined carefully. Here, we ignore that effect.) Fig. 13 indicates

that such phase shifts occur over a wide range of θ_i and ψ. Similarly, the observed pre-merger time delay for VIRGO relative to Livingston is about 14 ms, consistent with a small intrinsic phase shift and the 14 ms travel time between Livingston and VIRGO. The range of θ_i and ψ in Fig. 12 that meets these conditions is consistent with those noted in Fig 13. We see from Fig. 6 that these angles also fall in the range consistent with the observed *H/L* and *V/L* amplitude ratios. This argument illustrates how the combination of amplitude ratios, phase differences, and arrival-time delays can, in principle, constrain the source location, the orbital angle of inclination, and the polarization orientation angle.

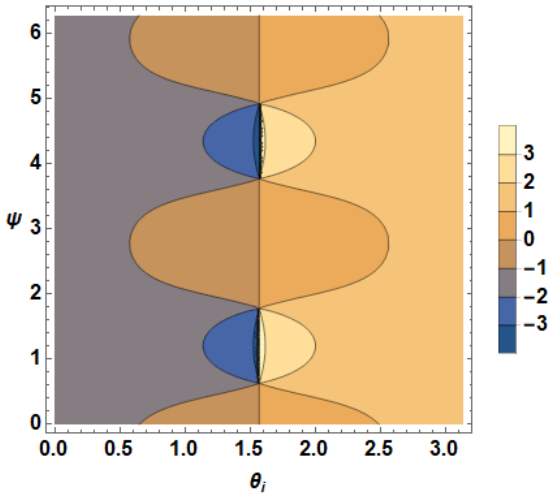

FIG. 14. A contour plot of the Hanford-Livingston vector model phase difference predictions (in radians) as a function of the orbital angle of inclination and the polarization orientation angle (both in radians). Same source location as Fig. 12.

Figure 14 shows the vector polarization model Hanford-Livingston phase difference for the source location used in Figs. 12 and 13. The pattern repeats for $\psi \to \psi + \pi$. Note that the vector model predicts phase shifts of about $\pm\pi$ over a much smaller range of angles compared to the tensor model predictions. Let us now examine how the phase shifts change for a location within the dark (red) oval in Fig. 3.

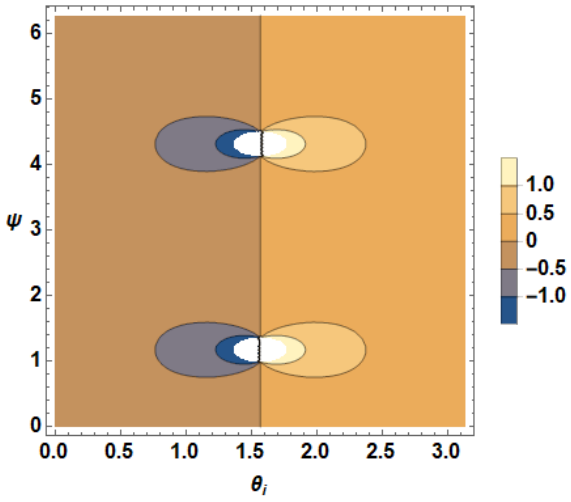

FIG. 15 Hanford-Livingston vector polarization phase difference in radians as a function of the orbital angle of inclination and the polarization orientation angle. Source location 40° S, 71.5° W (the same as Figs. 9-10).

The predictions of the vector polarization model for the Hanford-Livingston phase differences are plotted in Fig. 15 for a source location that gives vector model predicted amplitude ratios consistent with observations. Although the details differ, there are obvious similarities with the previous source location's phase differences. The tensor phase shifts for this source location (not shown) are similar to those displayed in Figs. 12 and 13.

Given the uncertainties in the amplitude ratios and in the observed phase shifts, it is difficult to draw definitive conclusions from the comparison of the predicted intrinsic phase shifts with the observations. We have seen that the phase differences in both the tensor and vector models, vary significantly with θ_i and ψ. In principle, detailed analysis of the phase shifts could lead to further restrictions on the range of orbital inclination angles and polarization orientation angles that are consistent with the observations, an issue we take up in the following section.

VIII. DISCUSSION

In this paper we have used an analysis employing specified GW source locations to determine the range of θ_i and ψ that gives results consistent with the observed GW170814 signal amplitude ratios. We then used those angles to examine intrinsic phase shifts between the signals from the three observatories. Our analysis focused on the GW170814 signals during the pre-merger inspiral phase of the binary motion. That focus allows us to ignore the complications that arise during the

merger and ring-down phases [37] due to strong space-time curvature and the concomitant scattering of the GWs in the near-field regime. From a GR point of view, the strong space-time curvature should lead to changes in the relative amplitudes and phases of the GW polarization modes. We could, in principle, use the amplitude ratios during the merger and ring-down phases to extract polarization information using the techniques described in this paper. However, the observations include only a few GW cycles during those phases and we might anticipate that the polarization amplitudes (and hence their relative phases) might change rapidly during merger and ring-down.

Unexpectedly, we find that a vector polarization model gives predictions consistent with observations in a band within or very close to the LIGO-VIRGO GW170814 source location 90% credible range. These location parameters are sensitive to the amplitude ratios, so the latter need to be determined as precisely as possible. Nonetheless, we have seen that analysis of the polarization modes via the GW detector signal amplitude ratios can in principle provide a test of how GR treats gravitational waves. Unfortunately, a detailed analysis [22] of the detection of gravitational wave transients like binary black hole coalescences indicates that for the GW170814 source location, the three LIGO-VIRGO observatories do not prove high discrimination among polarization modes. See Fig. 2 of Ref. [22].

The LIGO-VIRGO GW1709814 strain signal data [1] indicate that the amplitude ratios among the three observatories are approximately the same throughout the inspiral, merger, and ring-down stages. That result requires that the amplitude ratios and relative phases of the polarization modes remain the same throughout the GW event. As mentioned previously, one might expect that the ratios and phases should change during the merger and ring-down phases when the source space-time curvature becomes strong. Alternatively, if the orbital angle of inclination is near $\pi/2$, the plus mode for tensor polarization (or the *y* mode for vector polarization) for the associated GWs would have an amplitude much larger than the other mode and that would lead to approximately constant amplitude ratios and intrinsic phase shifts.

We note that tests of the polarization content of GWs can also be carried out with continuous wave GWs (if observed) [6,23]. Here "continuous" means that the GW signal duration is a significant fraction of a day, so the angles between the detector arms and the GW propagation direction and the polarization orientation change significantly during the observations. The most likely sources for continuous GWs whose frequencies fall within the LIGO-VIRGO detectors'

frequency bands are pulsars. The recent search [6] for such signals yielded a null result. A recent search for tensor, vector, and scalar polarizations in the stochastic GW background [38] also yielded a null result.

For other GW detection events, the inspiral analysis provided here can, under circumstances when the amplitude ratios are reasonably well-determined, provide an approximate range of orbital inclination and polarization orientation angles that might be helpful in setting parameters for a more detailed, full parameter numerical GR analysis of the event. We have also emphasized the importance of considering the full range of orbital inclination and polarization orientation angles in this kind of analysis.

Although the results presented here might tempt one to claim that GR's account of GWs is incomplete, we argue more conservatively that the observed GW signal amplitudes, which are difficult to measure precisely due to noise in the signals, particularly during the pre-merger inspiral, should be carefully measured before we can draw definitive conclusions about vector polarization contributions and their implications for post-GR physics.

Acknowledgements

The author thanks Nicolas Arnaud of the EGO/Virgo Outreach Team for directions to the gravitational wave detector location and orientation information. C. Mead and T. A. Moore provided several helpful discussions and comments. A. Svidzinsky, A. Weinstein, and M. Isi provided detailed comments and advice on a draft of this paper.

This research has made use of data, software and/or web tools obtained from the LIGO Open Science Center (https://losc.ligo.org), a service of LIGO Laboratory, the LIGO Scientific Collaboration and the Virgo Collaboration. LIGO is funded by the U.S. National Science Foundation. Virgo is funded by the French Centre National de Recherche Scientifique (CNRS), the Italian Istituto Nazionale della Fisica Nucleare (INFN) and the Dutch Nikhef, with contributions by Polish and Hungarian institutes.

References

[1] Abbott, B. P. *et al.*, Phys. Rev. Lett. **119**, 141101 (2017).

[2] T. Callister, S. Biscoveanu, N. Christensen, M. Isi, A. Matas, O. Minazzoli, T. Regimbau, M. Sakellariadou, J. Tasson, and E. Thrane, Phys. Rev. X **7**, 041058 (2017).

[3] C. Misner, K. Thorne, and J. A. Wheeler, *Gravitation* (W. H. Freeman, New York, 1973).

[4] T. A. Moore, *A General Relativity Workbook* (University Science Books, Mill Valley, California, 2013).

[5] M. Isi and A. J. Weinstein, LIGO-P1700276, arXiv: 1710.03794v1.

[6] Abbott, B. P, *et al.*, Phys. Rev. Lett. **120**, 031104 (2018).

[7] C. M. Will, arXiv: 1403.7377.

[8] E. Poisson and C. M. Will, *Gravity: Newtonian, Post-Newtonian, and Relativistic* (Cambridge University Press, Cambridge, 2014).

[9] D. M. Eardley, D. L. Lee, A. P. Lightman, R. V. Wagoner, and C. M. Will, Phys. Rev. Lett. **30**, 884 (1973).

[10] D. M. Eardley, D. L. Lee, and A. P. Lightman, Phys. Rev. D **8**, 3308 (1973).

[11] A. Nishizawa, A. Taruya, K. Hayama, S. Kawamura, and M. Sakagami, Phys. Rev. D **79**, 082002 (2009).

[12] K. Hayama and A. Nishizawa, arXiv: 1208.4596v2.

[13] K. Chatziioannou, N. Yunes, and N. Cornish, Phys. Rev. D **86**, 022004 (2012).

[14] M. Isi, M. Pitkin, and A. J. Weinstein, Phys. Rev. D **96**, 042001 (2017).

[15] A. A. Svidzinsky, Phys. Scr. **92**, 125001 (2017).

[16] C. Mead, arXiv: 1503.04866v1.

[17] R. C. Hilborn, Am. J. Phys. **86**, 186 (2018).

[18] Abbott, B. P. *et al.*, Phys. Rev. Lett. **116**, 221101 (2016).

[19] S. Fairhurst, arXiv: 1712.04724v1.

[20] A. A. Svidzinsky, arXiv:1712.07181v1.

[21] S. Klimenko, S. Mohanty, M. Rakhmanov, and G. Mitselmakher, Phys. Rev. D **72**, 122002 (2005).

[22] S. Klimenko, G. Vedovato, M. Drago, *et al.*, Phys. Rev. D **93**, 042004 (2016).

[23] M. Isi, A. J. Weinstein, C. Mead, and M. Pitkin, Phys. Rev. D **91**, 082002 (2015).

[24] L. Fesik, arXiv:1706.09505v1.

[25] B. Allen, arXiv:1801.04800v1.

[26] T. A. Apostolatos, C. Cutler, G. J. Sussman, and K. S. Thorne, Phys. Rev. D **49**, 6274 (1994).

[27] I. Di Palma and M. Drago, arXiv: 1712. 05580 [astro-ph. IM].

[28] LIGO-VIRGO Collaboration, *LIGO Interferometric Detector Constants*, https://losc.ligo.org/s/param/position.txt (2016).

[29] W. G. Anderson, P. R. Brady, J. D. E. Creighton, and É. É. Flanagan, Phys. Rev. D **63**, 042003 (2001).

[30] W. Anderson, P. Brady, D. Chin, J. Creighton, K. Riles, and J. Whelan, *Beam Pattern Response Functions and Times of Arrival for Earthbound Interferometer*, LIGO-T010110-00-Z (2009).

[31] LIGO-VIRGO Collaboration, *GW170814 Fact Sheet*, https://losc.ligo.org/events/GW170814/ (2017).

[32] Abbott, B. P. *et al.*, Phys. Rev. Lett. **119**, 161101 (2017).

[33] A. A. Svidzinsky and R. C. Hilborn, in preparation (2018).

[34] R. H. Price and G. Khanna, arXiv: 1607.04226v2.

[35] L. E. Kidder, Phys. Rev. D **52**, 821 (1995).

[36] S. Vitale, Phys. Rev. D **94**, 121501 (2016).

[37] J. Veitch, V. Raymond, B. Farr, *et al.*, Phys. Rev. D **91**, 042003 (2015).

[38] Abbott, B. P. *et al.*, arXiv: 1802.10194.